X-ray diffraction assisted spectroscopy of Rydberg states

AIP | The Journal of Chemical Physics

X-ray diffraction assisted spectroscopy of Rydberg states

Adam Kirrander

Citation: J. Chem. Phys. **137**, 154310 (2012); doi: 10.1063/1.4757913
View online: http://dx.doi.org/10.1063/1.4757913
View Table of Contents: http://jcp.aip.org/resource/1/JCPSA6/v137/i15
Published by the American Institute of Physics.

X-ray diffraction assisted spectroscopy of Rydberg states

Adam Kirrander[a)]
ITAMP, Harvard-Smithsonian Center for Astrophysics, Cambridge, Massachusetts 02138, USA

(Received 5 July 2012; accepted 24 September 2012; published online 18 October 2012)

X-ray diffraction combined with conventional spectroscopy could provide a powerful means to characterize electronically excited atoms and molecules. We demonstrate theoretically how x-ray diffraction from laser excited atoms can be used to determine electronic structure, including angular momentum composition, principal quantum numbers, and channel populations. A theoretical formalism appropriate for highly excited atoms, and easily extended to molecules, is presented together with numerical results for Xe and H atoms. © *2012 American Institute of Physics*. [http://dx.doi.org/10.1063/1.4757913]

I. INTRODUCTION

In recent years there has been a rapid development of new x-ray free-electron lasers (FEL), including the Linac Coherent Light Source (LCLS) at Stanford, the European X-ray Free-Electron Laser (XFEL) in Hamburg and other facilities currently under construction. The high intensity x-ray radiation from these new sources has many interesting applications, including crystal-free diffraction imaging of biomolecules.[1,2] The combination of high intensity and short pulse duration offered by the FELs is also ideal for diffraction using elastic scattering of x-ray photons from transient species in the gas phase, including electronically excited states in atoms and molecules. To date, such studies were only possible in rare species with extremely long-lived excited electronic states.[3]

The potential benefits of such diffraction studies were first pointed out by Wilson and collaborators in their pioneering work on time-resolved x-ray diffraction.[4,5] Now, as such experiments are becoming increasingly more likely, we present a unified theoretical framework for both diffraction and spectroscopy of excited states based on multichannel quantum defect theory (MQDT). We propose that diffraction-based techniques could become an important complement to more conventional spectroscopic techniques. Modern laser spectroscopy can determine the energy levels, transition intensities and line shapes of atoms, and molecules with high precision,[6,7] but analysis of the spectra is often difficult and requires complicated theoretical models. The complementary spatial information provided by diffraction, which directly probes the electron density of the sample, could resolve ambiguities in spectroscopic assignments and greatly simplify the analysis of spectra, as well as provide an independent check on prevailing theory.

In this paper, we examine in detail the diffraction from highly excited electronic states (also known as Rydberg states) in simple and complex atoms. We find that angular momentum coupling between Rydberg electrons and the core lead to robust signatures in the diffraction patterns, and that in some instances it may be experimentally advantageous to study the Rydberg electron indirectly, via diffraction from the positive core. We also show, more specifically, how the diffraction pattern contains information on the angular momentum composition, the radial wave functions, and the relative channel populations for an excited electronic state. In molecules, Rydberg states can provide a signature of the molecular structure,[8] not dissimilar to how photoelectron angular distributions give detailed information on atomic and molecular states.[9] In ultrafast dynamics, there are interesting reactions that proceed through Rydberg states,[10] where unambiguous spectroscopic assignment of transient intermediates is difficult and may be significantly aided by a diffraction signature. Again, there is an analogy to how time-resolved photoelectron spectroscopy is used to study dynamics.[11]

A schematic representation of the proposed experiment is shown in Figure 1. The setup is very similar to what has already been used in time-dependent x-ray diffraction experiments at third generation synchrotrons (see, e.g., Ref. 12). This paper is structured as follows. In Sec. II we present the theoretical description of highly excited states using MQDT, which we use to calculate the electron density and to derive expressions for the elastic x-ray scattering (diffraction). In Sec. III we apply the theory to calculate wave functions and associated electron densities for excited states in H and Xe atoms. The resulting diffraction patterns are analyzed in Sec. IV and experimental considerations are given in Sec. V.

II. THEORY

A. Theoretical description of highly excited states

Highly excited atomic and molecular states can be described by MQDT,[13–16] which regards Rydberg states as consisting of an excited electron scattering from a positive ion core. Outside the core, the Rydberg electron moves in a Coulomb potential and occupies a large volume of space. When it enters the core, thereby forming a compact collision complex, interactions with the core electrons and the nucleus lead to exchange of energy and angular momentum. The effect of these interactions on the Rydberg electron wave function located outside the core can be summarized in terms of a short-range scattering matrix. This scattering matrix can be calculated by the R-matrix method,[17] or by fitting to

[a)]Electronic mail: adam.kirrander@gmail.com.

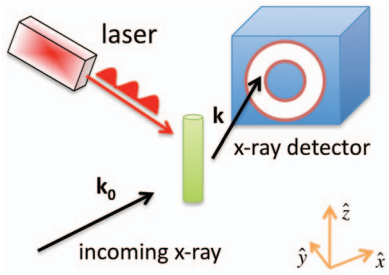

FIG. 1. Schematic of the proposed experiment. The sample atoms are excited by a laser with planar polarization along the $\hat{z}$-axis. The direction of the incoming x-ray beam is $\mathbf{k}_0$, which defines the $\hat{x}$-axis, and the diffracted x-rays are measured along $\mathbf{k}$. The direction of $\mathbf{k}$ is expressed in spherical angles θ, ϕ relative the incoming x-ray beam $\mathbf{k}_0$.

ab initio electronic structure calculations or experimental Rydberg spectra.[14] Below, we present the mathematical form of the Rydberg wave functions as obtained by MQDT for bound states.

Using the real form of the scattering matrix, $\mathbf{K}$, the scattering wave function $\mathbf{\Phi}$ for the Rydberg state is a $N_c \times N_c$ matrix with elements,

$$\mathbf{\Phi}_{jk} = |\Psi_j^+\rangle \left[\frac{1}{r} Y_{l_j m_j}(\vartheta, \varphi)\{f_j(r)\delta_{jk} - g_j(r)\mathbf{K}_{jk}\}\right], \quad (1)$$

where the square brackets contain the Rydberg electron wave function outside the core, with $f_j(r)$ and $g_j(r)$ the radial Coulomb functions in channel j, and $Y_{l_j m_j}(\vartheta, \varphi)$ the corresponding orbital angular momentum spherical harmonic. The positive ion core wave function, $|\Psi_j^+\rangle$, contains all degrees of freedom and factors not made explicit in Eq. (1). The scattering of the Rydberg electron from the core introduces phase shifts into the channel components of the outer electron wave function by mixing irregular (cos -like) components $g_j(r)$ with the regular (sin -like) components $f_j(r)$ via the $\mathbf{K}$ matrix. Each of the N_c scattering channels, indexed by j, corresponds to a particular configuration of the core and the Rydberg electron. The columns of matrix $\mathbf{\Phi}$ in Eq. (1) form N_c linearly independent wave functions. To find bound states, we form a linear superposition Ψ

$$\Psi = \mathbf{\Phi} Z, \quad (2)$$

where the linear expansion coefficients in the column vector Z are determined to yield a bound wave function Ψ that vanishes exponentially in each channel when $r \to \infty$, as the physical boundary conditions require. Such bound states can only be found at discrete energies, given by[13,14]

$$(\mathbf{K} + \tan\beta)\, Z = 0, \quad (3)$$

where the diagonal matrix $\tan\beta$ is a function of the accumulated radial phase β in each channel. Bound states appear as a result of resonances in the external Coulomb potential (via the accumulated phase β). The short-range scattering matrix $\mathbf{K}$ remains nearly constant between resonances.

The end result is a Rydberg state wave function which can be written in the form,

$$\Psi = \sum_{j=1}^{N_c} |\Psi_j^+\rangle \left[\frac{1}{r} Y_{l_j m_j}(\vartheta, \varphi) R_j(r)\right], \quad (4)$$

where the sum runs over the N_c channels. The square bracket contains the Rydberg electron wave function. The radial wave function, $R_j(r)$, is a sum of $f_j(r)\delta_{jk} - g_j(r)\mathbf{K}_{jk}$ components from Eq. (1), multiplied by the weights Z from Eq. (2). Green's theorem makes it possible to normalize the Rydberg wave function without knowing the internal $r < r_c$ part explicitly,[14,15,18] and antisymmetrization of the total Rydberg wave function is not required due to the small overlap of the core and Rydberg electron wave functions.[17] In the next section, wave functions of the form in Eq. (4) are used to calculate electron densities.

B. Electron density from Rydberg wave functions

The x-rays diffract from the total electron density, obtained by integrating out all but one electronic coordinates in the probability density for the system. The total N electron density for a Rydberg state, $\rho_{tot}^{(N)}$, has three components,

$$\rho_{tot}^{(N)}(\mathbf{r}) = \rho_{r>r_c}^{(1)}(\mathbf{r}) + \rho_{r<r_c}^{(N-1)}(\mathbf{r}) + P_{r<r_c}\, \rho_{r<r_c}^{(N)}(\mathbf{r}), \quad (5)$$

where $\rho_{r>r_c}^{(1)}$ is the Rydberg electron density, $\rho_{r<r_c}^{(N-1)}$ is the $N-1$ electron density of the ion core, and $\rho_{r<r_c}^{(N)}$ is the N electron density of the collision complex. The subscripts indicate the radial range of each component with r_c the radius of the collision complex, while the superscripts correspond to the number of electrons in each component. The density coordinate is $\mathbf{r} = (r, \vartheta, \varphi)$.

Although the collision complex density, $\rho_{r<r_c}^{(N)}$, could be calculated by the R-matrix method,[17] it is disregarded in the present treatment because it changes very little going from one Rydberg state to another. Accounting for state-specific changes in the dipole transition moment, it gives a constant background that can be subtracted. In addition, the prefactor, $P_{r<r_c}$, in Eq. (5) is small. In this paper we focus on the two most variable components of the wave function, corresponding to the terms in Eq. (5) that originate from the Rydberg wave function in Eq. (4), i.e., the diffuse Rydberg electron, $\rho_{r>r_c}^{(1)}$, and the compact core, $\rho_{r<r_c}^{(N-1)}$.

The Rydberg electron density outside the core, $\rho_{r>r_c}^{(1)}$, is given by

$$\rho_{r>r_c}^{(1)}(\mathbf{r}) = \frac{1}{r^2} \sum_{j=1}^{N_c} |Y_{l_j m_j}(\vartheta, \varphi)|^2 |R_j(r)|^2, \quad (6)$$

where we integrate out the $N-1$ core electrons such that $\langle \Psi_j^+ | \Psi_{j'}^+ \rangle = \delta_{jj'}$. The total probability that the Rydberg electron resides outside the core is

$$P_{r>r_c} = \int_{r>r_c} \rho_{r>r_c}^{(1)}(\mathbf{r})\, d\mathbf{r} = \sum_{j=1}^{N_c} \int_{r>r_c} |R_j(r)|^2\, dr, \quad (7)$$

where we use the orthonormality of the spherical harmonics Y_{lm}. The probability that the Rydberg electron is inside the core is $P_{r<r_c} = 1 - P_{r>r_c}$ and appears in Eq. (5).

The electron density from the core $N-1$ electron wave function is given by integrating out the Rydberg electron and

all electrons in the core except one,

$$\rho_{r<r_c}^{(N-1)}(\mathbf{r}) = \sum_{j=1}^{N_c} \rho_{j,r<r_c}^{(N-1)}(\mathbf{r}) \int_{r>r_c} |R_j(r)|^2 \, dr, \tag{8}$$

where $\rho_{j,r<r_c}^{(N-1)}$ is the electron density for the core in the electronic state corresponding to channel j. No cross-terms appear in Eq. (8) since each channel has different set of angular and spin quantum numbers. We assume that the core density for each channel, $\rho_{j,r<r_c}^{(N-1)}$, can be written as a radial density function multiplied by an orbital angular momentum,

$$\rho_{j,r<r_c}^{(N-1)} = \frac{1}{r^2} |Y_{l_j m_j}(\vartheta, \varphi)|^2 |\mathcal{R}_j(r)|^2. \tag{9}$$

For a complex atom, we must ensure that the total wave function has the correct total angular momentum, which leads to a weighted sum over different quantum numbers m in each channel. This is discussed for the case of Xe atoms at the end of Sec. III. This leads to spatial correlation between the core wave function and that of the Rydberg electron which makes it possible to use diffraction from the core to infer information about the Rydberg electron (see discussion in Sec. IV B).

C. X-ray diffraction

We now turn to the x-ray diffraction from the electron density calculated in Sec. II B. Because the lifetimes of Rydberg states are significantly longer than the duration of the x-ray probe pulse,[16] we can treat the problem as diffraction of a continuous x-ray beam from a static target.[19,20] Within the first Born approximation the N-electron diffraction operator $L(\mathbf{s})$ for x-rays is (see, e.g., Ref. 21)

$$L(\mathbf{s}) = \sum_{i}^{N} e^{\imath \mathbf{s} \mathbf{r}_i}, \tag{10}$$

where the vector $\mathbf{s} = \mathbf{k}_0 - \mathbf{k}$ is the difference between the incident wave vector $\mathbf{k}_0$ and the scattered wave vector $\mathbf{k}$, with $k_0 = E/\hbar c$ for x-ray photon energy E and c the speed of light. For off-resonant x-ray photon energies it is sufficient to discuss elastic diffraction, $k_0 = k$. The diffraction amplitude, also known as the atomic form factor, $f(\mathbf{s})$, from a bound and normalized N electron wave function $\phi(\mathbf{r}_1, \ldots, \mathbf{r}_N)$ is

$$f(\mathbf{s}) \propto \langle \phi | L(\mathbf{s}) | \phi \rangle = \int \rho_{tot}^{(N)}(\mathbf{r}) e^{\imath \mathbf{s} \mathbf{r}} d\mathbf{r}, \tag{11}$$

where we make use of the fact that the electrons are indistinguishable. From Eq. (11) it is clear that it is the N electron density, $\rho_{tot}^{(N)}$, that diffracts the x-rays. Experimentally, the intensity of the diffracted signal is proportional to $|f(\mathbf{s})|^2$. For an atom it is reasonable (see Eqs. (6) and (9)) to write the electron density $\rho(\mathbf{r})$ as a sequence of radial densities, $|R_j(r)|^2/r^2$, multiplied by corresponding angular densities given by the spherical harmonics, $|Y_{l_j m_j}(\vartheta, \varphi)|^2$. This gives electron densities of the form,

$$\rho(\mathbf{r}) = \frac{1}{r^2} \sum_{j=1}^{N_c} |Y_{l_j m_j}(\vartheta, \varphi)|^2 |R_j(r)|^2. \tag{12}$$

To solve the integral for $f(\mathbf{s})$ in Eq. (11) we expand the plane wave in spherical partial waves,

$$e^{\imath \mathbf{s} \mathbf{r}} = 4\pi \sum_{l=0}^{\infty} \sum_{m=-l}^{+l} \imath^l Y_{lm}^*(\vartheta_s, \varphi_s) j_l(sr) Y_{lm}(\vartheta, \varphi), \tag{13}$$

where $j_l(sr)$ are the spherical Bessel functions. Inserting this expansion and the generic electron density from Eq. (12) into Eq. (11), we obtain

$$f(\mathbf{s}) = 4\pi \sum_{j}^{N_c} \sum_{l=0}^{2l_j} \imath^l Y_{lm}^*(\vartheta_s, \varphi_s) \; Q_{l_j m_j lm} \; B_{jl}(s), \tag{14}$$

which is the main result of this section. The factor $Q_{l_j m_j lm}$ corresponds to the integral over three spherical harmonics and is zero unless $m = 0$ and $0 \le l \le 2l_j$. According to the Wigner-Eckart theorem $Q_{l_j m_j lm}$ is

$$Q_{l_j m_j lm} = \sqrt{\frac{(2l_1 + 1)(2l_2 + 1)}{4\pi(2l_3 + 1)}} \; \langle l_j l 00 | l_j 0 \rangle \; \langle l_j l m_j m | l_j m_j \rangle. \tag{15}$$

The factor $B_{jl}(s)$ in Eq. (14) is a Bessel transform of the radial probability density,

$$B_{jl}(s) = \int |R_j(r)|^2 j_l(sr) \, dr, \tag{16}$$

which essentially amounts to a Fourier transform of the radial density. In the proposed experimental setup shown in Figure 1, the atoms are excited by a laser with planar polarization along the $\hat{z}$-axis, and probed by an x-ray beam with wave vector $\mathbf{k}_0$ along the $\hat{x}$-axis. The diffracted x-ray beam is measured by a detector positioned in the direction $\mathbf{k}$, defined by spherical angles θ, ϕ relative the direction of $\mathbf{k}_0$. We, therefore, calculate the form factor $f(\mathbf{s})$ in Eq. (14) as a function of θ, ϕ, since $\mathbf{s} = \mathbf{s}(\theta, \phi)$. In this setup, the amplitude of $\mathbf{s}$ only depends on θ, i.e., $s = 2k_0 \sin(\theta/2)$. Consequently, B_{jl} in Eqs. (14) and (16) only depends on the radial diffraction angle θ and all information about the radial wave function is contained in the θ dependence of the scattering pattern. To avoid confusion, note the difference between the diffraction angles θ, ϕ and the angles ϑ, φ used in the spherical harmonics in the wave functions. These latter angles have the standard definition relative the laboratory frame coordinate system, with ϑ forming an angle with the $\hat{z}$-axis.

III. NUMERICAL CALCULATION OF RYDBERG WAVE FUNCTIONS

In order to calculate the actual diffraction pattern from electronic Rydberg states, we need to calculate the wave functions which in turn will give us the electron density. Below we discuss aspects of calculating Rydberg wave functions in two model systems, H and Xe atoms. In both cases, the calculated energy levels agree well with experimental levels.

For H atoms, the wave functions are known analytically and have the form,

$$\Psi_n(\mathbf{r}) = r^{-1} R_n(r) Y_{LM}(\vartheta, \varphi), \tag{17}$$

where Y_{LM} is a spherical harmonic and the bound energies are $E_n = -0.5/n^2$ in atomic units. Figure 2(a) shows the radial

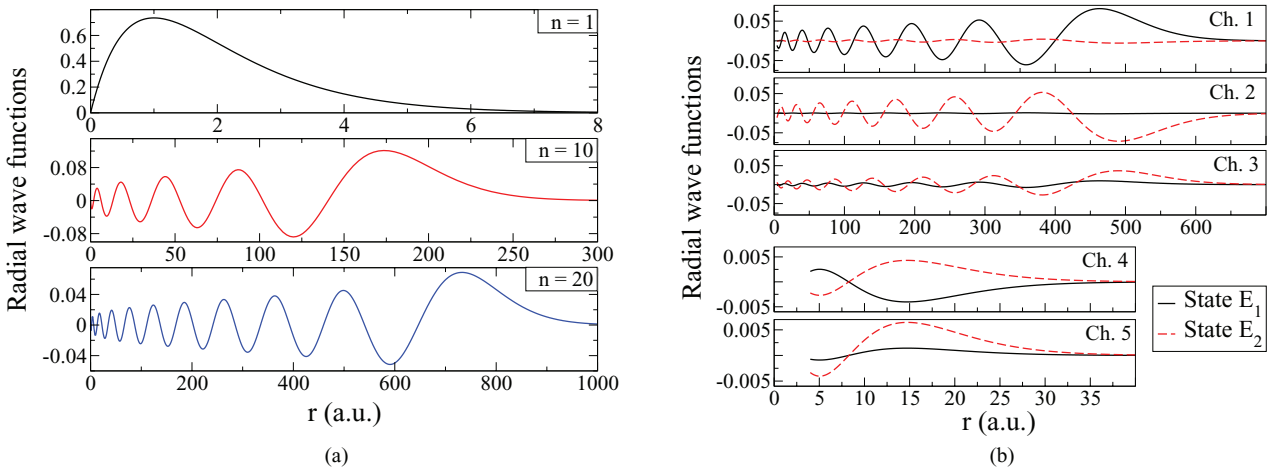

FIG. 2. Radial Rydberg electron wave functions $R_j(r)$ for H and Xe atoms. The classical turning point, r_{tp}, for the wave functions scales as $r_{tp} = 2n^2$. The wave functions are bound-state normalized. (a) (H atom) Radial wave functions for $L = 0$ ($M = 0$) and principal quantum numbers $n = 1$ (top), $n = 10$ (middle), and $n = 20$ (bottom). (b) (Xe atom) Radial electronic Rydberg wave functions for states E_1 and E_2 in channels $j = 1$–5 (see Table I). The core is contained inside the volume $r_c < 5$ a.u. The principal quantum numbers in the channels $j = 1$–3 are $n \approx 20$, and $n \approx 5$ in $j = 4$–5.

wave functions for three s orbital states ($L = 0$) with principal quantum numbers $n = 1$, 10, and 20.

In Xe, we regard two adjacent bound Rydberg states with total angular momentum $J = 1$. The two states, referred to as E_1 and E_2, are listed by NIST[22] and appear at energies 97 405.6 cm^{-1} and 97 430.0 cm^{-1}. At these energies, Xe has five dipole-allowed Rydberg channels, given in Table I and identified by the state of the core, Xe^+, and that of the Rydberg electron. The calculated character for each state is given in Table I. Although the states are adjacent, there is a significant difference in their character, with channel $j = 1$ dominating E_1 while E_2 is dominated by $j = 2$–3. The calculations use the **K** matrix and dipole transition moments from the relativistic spin-orbit coupled MQDT calculations by Johnson *et al.*[23] The radial Rydberg electron wave functions shown in Figure 2 are calculated by the Milne method[24] and the radial wave functions for the Xe^+ core states are estimated from published form factors for Xe (NIST[25]).

The electron density in the yz-plane for the Rydberg electron in state E_1 is shown in Figure 3 for channels $j = 1$, 3, and 5. The radial electron density (including the nodal pattern) is determined by the radial wave function, while the spatial angular density distribution depends on the orbital angular momentum. Channels $j = 1$ and 4 both have isotropic electron density ($l = 0$, see Table I), while the remaining channels are anisotropic. To calculate the electron density we require the expansion of orbital angular momentum functions that accompany each channel. We write the angular momentum states as $|JM\rangle$, with angular momentum J and projection M. Single photon excitation from the ground state $|00\rangle$ wave function with linearly polarized light gives a total excited wave function $|10\rangle$. This excited state is described using jj-coupling between the Rydberg electron and the core,

$$|10\rangle = \sum_{M_c+m_e=0} \langle J_c j_e M_c m_e|10\rangle \; |J_c M_c\rangle|j_e m_e\rangle. \tag{18}$$

For each channel j, the core momenta J_c, L, and S, and the Rydberg electron momenta j_e, l, and s are given in Table I. To find the expansion of orbital angular states for the Rydberg electron, we expand the Rydberg electron angular momentum

$$|j_e m_e\rangle = \sum_{m_l+m_s=m_e} \langle l s m_l m_s|j_e m_e\rangle \; |l m_l\rangle|s m_s\rangle \tag{19}$$

with $|m_l| \le l$ and $|m_s| \le s$ according to the triangle inequality. Inserting Eq. (19) into Eq. (18) gives for channel j that

$$|10\rangle = \sum_{m_l,m_s} \langle J_c j_e M_c m_e|10\rangle \; \langle l s m_l m_s|j_e m_e\rangle|J_c M_c\rangle|l m_l\rangle|s m_s\rangle, \tag{20}$$

where m_e is defined as $m_e = m_l + m_s$, $M_c = -m_e$, $|M_c| \le J_c$, $|m_l| \le l$, and $|m_s| \le s$. As a consequence of Eq. (20), the radial wave functions $R_j(r)$ in Eq. (4) will be multiplied not by a single spherical harmonic $Y_{l_j m_j}$ function, but by a weighted sum of spherical harmonics with the same l_j but different m_j. The same procedure gives the expansion of orbital angular momentum states of the core. It should be noted that the angular momentum distribution (and hence the spatial wave function) of the core and the Rydberg electron are thus intrinsically linked, meaning that the one can be inferred from the other for instance via their diffraction pattern.

TABLE I. The calculated character of the two bound Xe states E_1 and E_2 given as the % population in each channel. The three channels $j = 1$–3 correspond to the ground electronic state of the core and $j = 4$–5 to the first excited state. Core states are given as $^{2S+1}L_{J_c}$, where J_c is the total, L is the orbital and S is the spin angular momentum of the core. The Rydberg electron is given as l_{j_e}, where l is the electron orbital and j_e is the total electron angular momentum, including the electron spin.

Channel (j)	1	2	3	4	5
Core (Xe^+)	$^2P_{3/2}$	$^2P_{3/2}$	$^2P_{3/2}$	$^2P_{1/2}$	$^2P_{1/2}$
Rydberg electron	$s_{1/2}$	$d_{3/2}$	$d_{5/2}$	$s_{1/2}$	$d_{3/2}$
Population E_1 (%)	98	0.03	1.5	0.02	0.002
Population E_2 (%)	1	79	21	0.02	0.04

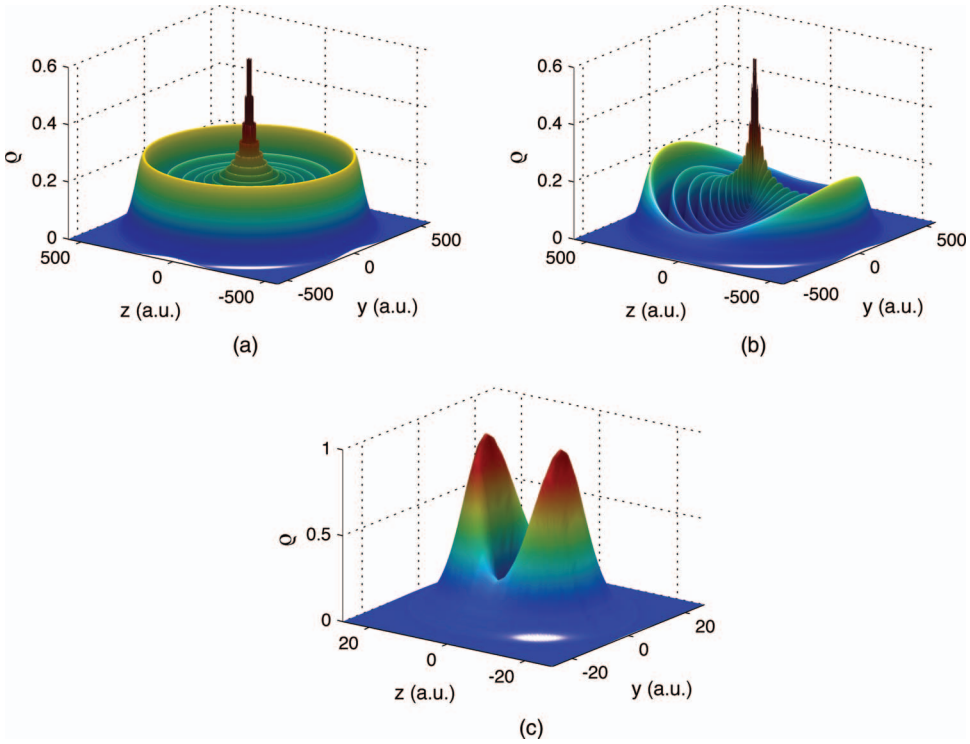

FIG. 3. The Rydberg electron density in the yz-plane for state E_1 in Xe (see Table I). (a)–(c) show channels $j = 1$, 3, and 5, respectively. The density is isotropic in channels $j = 1$, 4, and anisotropic in the other channels. The electron density has been multiplied by the radius r, and re-normalized so that the maximum value is 1 in each channel in order to aid visualization. (a) Channel $j = 1$. (b) Channel $j = 3$ (and channel $j = 2$ by a 90° rotation around the perpendicular $\hat{x}$-axis). (c) Channel $j = 5$ (note that $j = 4$ is similar in size and nodal pattern, but is isotropic like $j = 1$).

IV. RESULTS

A. Diffraction from H atoms

In order to establish the basic properties of diffraction from Rydberg states, we examine the x-ray diffraction from excited H atoms. We use Eq. (14) to calculate the diffraction form factor, $|f(\theta, \phi)|^2$, with wave functions determined by Eq. (17) and do not at this stage take into account the excitation process or the optical selection rules. The orbital angular momentum gives a signature in the diffraction pattern which is quite insensitive to the matching between the x-ray probe wavelength and the spatial dimensions of the electron density. In contrast, in order to extract the maximum information about the radial electron wave function from the diffraction pattern, the wavelength must be matched to the radial dimensions.

Figure 4 demonstrates the strong signature of the orbital angular momentum in the diffraction pattern. The left-hand column shows contour plots of the diffraction pattern, $|f(\theta, \phi)|^2$, from H atoms with different orbital angular momentum $L = 0$, 1, and 2 (i.e., s, p, and d orbitals), but the same quantum numbers $n = 10$ and $M = 0$. The righthand column in the figure shows the electron density of each of these states. Although the radial wave functions are almost identical, the different angular spatial density leads to notably different diffraction patterns. The diffraction pattern for the isotropic s state is independent of ϕ, while both p and d states have a distinct ϕ dependence. The diffraction pattern is also

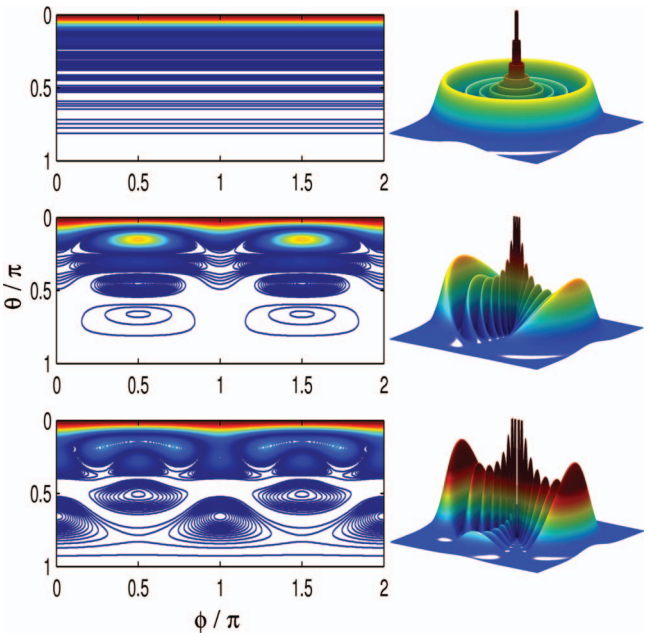

FIG. 4. Diffraction patterns from states in H atoms with different angular momentum L, but otherwise identical quantum numbers $n = 10$ and $M = 0$. The angular momenta $L = 0$ (top), $L = 1$ (middle), and $L = 2$ (bottom) correspond to s, p, and d orbitals. The righthand column shows the electron density for each state in the yz-plane (see Figure 3 for technical details) and the lefthand column shows contour plots of the diffraction, $|f(\theta, \phi)|^2$, along the radial θ and angular ϕ coordinates (see Figure 1). The x-ray wavelength is $\lambda = 150$ a.u. (156 eV) and the incoming x-ray is aligned with the $\hat{x}$-axis. Note that background diffraction from, e.g., ground state atoms is not included.

sensitive to the direction of the incoming x-ray for a fixed orientation of the excitation laser. For instance, the anisotropy of the p and d orbitals with $M = 0$ in Figure 4 does not appear if the incoming x-ray beam is aligned with the $\hat{z}$-axis. This could be used to determine the value of quantum number M, when relevant.

In contrast, to extract maximum detail about the radial wave function from the diffraction pattern, the incoming x-ray photon wavelength $\lambda = 2\pi/k_0$ must match the spatial dimensions of the wave function. The radial diffraction pattern is determined by the factor $B_{jl}(s)$ in Eq. (16), with the range of s sampled by a particular k_0 being $0 \leq s \leq 2k_0$, with the value of s a function of the radial diffraction angle θ (see Sec. II C). Figure 5 shows the radial diffraction pattern, $|f(\theta)|^2$, for a $n = 10$ and $L = 0$ wave function for a range of different x-ray wavelengths λ given in atomic units (1 a.u. $\approx$ 0.53 Å) and in eV. It can be seen that the most detail is retained at $\lambda = 75$ a.u. (312 eV), which matches the dimensions of the radial wave function reasonably well. Since the classical turning point ($\approx$size) of the Coulomb wave functions is $r_{tp} = 2n^2 = 200$ a.u. and the nodes are spaced by approximately $\triangle r \approx r_{tp}/n = 20$ a.u. we expect the most useful diffraction patterns to occur for $20<\lambda<200$ a.u. (1.2 keV–117 eV). Indeed, in Figure 5 the probe x-ray wavelengths $\lambda = 75$ a.u. (312 eV) and 150 a.u. (156 eV) retain the greatest amount of detail. If λ is too short, all the diffraction signal is observed at small angles θ, as can be seen for $\lambda = 5$ a.u. (4.7 keV) in Figure 5, and if λ is too long, most oscillations in the diffraction are lost, as can be seen for $\lambda = 600$ a.u. (39 eV). There are a few general remarks to be made. In the Bessel transform of the radial density in Eq. (16), large features in real space r will give rise to small features in reciprocal space s and vice versa, and periodic structures (notably the nodes) in the wave function will give corresponding periodic structures in reciprocal s space. Also, all form factors f have the value N in the direction $\theta = 0$, where N is the number of electrons, since $s = 0$ in Eq. (11).[21]

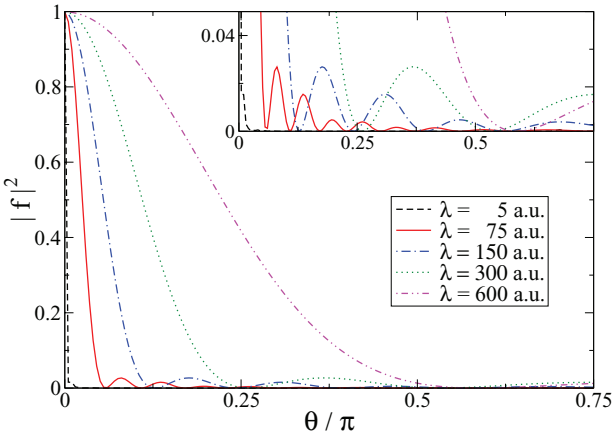

FIG. 5. Diffraction signal as function of the radial angle θ for different x-ray probe wavelengths λ from H atoms with angular momentum $L = M = 0$ and principal quantum number $n = 10$ (classical turning point at 200 a.u.). The probe wavelength λ needs to be matched to the spatial dimensions of the radial wave function to avoid loss of information. The range $\lambda = 5$–600 a.u. corresponds to photon energies 4.7 keV–39 eV. Details of the diffraction pattern are shown in the insert.

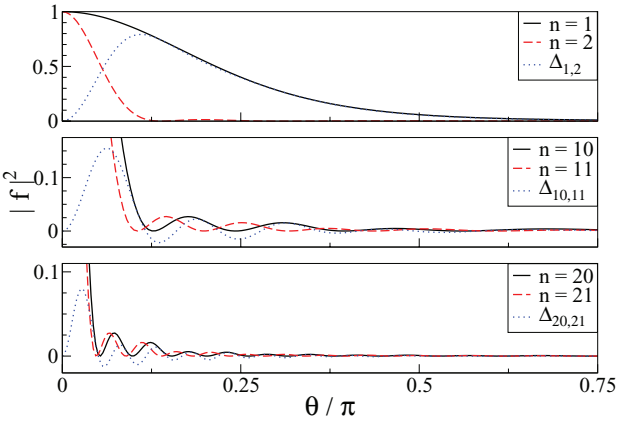

FIG. 6. The radial diffraction signal as a function of principal quantum number n. The greatest difference is between $n = 1$ and $n = 2$ (top), but it remains significant for $n = 10$ and $n = 11$ (middle) and even for $n = 20$ and $n = 21$ (bottom). In each case, the x-ray wavelength λ is chosen to match the size of the electronic state ($\lambda = 6$ a.u. at the top, $\lambda = 150$ a.u. in the middle and $\lambda = 250$ a.u. at the bottom, corresponding to photon energies 3.9 keV, 156 eV, and 94 eV, respectively). Angular quantum numbers are $L = M = 0$, and the difference signal $\Delta_{n,n+1}$ is included as a dotted line in each plot.

For appropriately chosen x-ray wavelengths λ, the radial diffraction pattern along θ can be used to distinguish states with different principal quantum numbers and hence different radial wave functions. In Figure 6 the radial form factor $|f(\theta, \phi)|^2 = |f(\theta)|^2$ is compared for three sets of nearest-neighbour wave functions with principal quantum numbers $(n, n + 1)$ for $n = 1$, 10, and 20. For each set, an appropriate x-ray wavelength is chosen. We see that there is a strong difference in diffraction pattern between $n = 1$ and its nearest neighbour $n = 2$. Neither $n = 1$ nor $n = 2$ are truly Rydberg states, but the difference in diffraction pattern persists for higher n states, although it does become weaker. As shown in the figure, there is still a discernible difference between $n = 20$ and $n = 21$. In principle, this difference signal could be enhanced by measuring the diffraction at several different wavelengths λ.

B. Diffraction from Xe atoms

We now turn to diffraction from Rydberg states in complex atoms such as Xe. The main difference compared to the simple H atom is that the additional electrons in the core also diffract, and that coupling between the Rydberg electron and the core leads to composite (multichannel) Rydberg wave functions. Here, adjacent electronic states can have dramatically different character, giving strong difference signatures in the diffraction pattern. The electronic structure of the Xe ground state is $[\mathrm{Kr}]4d^{10}5s^25p^6$, with 18 outer electrons. In a Rydberg state, one of these outer electrons is excited to a high-lying electronic state. Angular momentum coupling and conservation of total angular momentum ensures that the spatial anisotropy of the Rydberg wave functions is matched by anisotropy of the remaining 17 outer electrons. One can, therefore, expect anisotropic diffraction signals from the Rydberg electron ($f_0^2 \sim 1$) as well as the outer electrons in the core ($f_0^2 \sim 10^2$), while the electrons in the closed inner shell generally remain unaffected by the excitation and give rise

to isotropic diffraction ($f_0^2 \sim 10^3$). The electron density for Rydberg states in Xe consists of the three components listed in Eq. (5), namely the core, the Rydberg electron, and the collision complex. As discussed in Sec. II B, the collision complex component can be excluded to a good approximation, which leaves a wave function in the format given by Eq. (4). We calculate the total diffraction pattern $|f(\theta, \phi)|^2$ using Eq. (14). Although we include the excitation process using the dipole transition moments from Ref. 23, the background diffraction from the ground state Xe atoms is completely isotropic and we therefore show the excited state diffraction only, rather than the difference diffraction signal ("laser on" – "laser off") that would be measured in an actual experiment.[19,26]

Figure 7 shows contour plots of the total diffraction pattern, $|f(\theta, \phi)|^2$, from the states E_1 and E_2 presented in Sec. III at two different x-ray probe wavelengths. The large difference between the diffraction patterns for the two adjacent states, regardless of the probe wavelength λ, illustrates how the diffraction patterns can provide specific fingerprints of each state, and therefore an unambiguous method to distinguish and identify different states in the spectrum. The strong angular (ϕ) signature in the diffraction patterns originates from the change in spatial angular distribution associated with the change in character between the two states (see Table I).

By adjusting the probe wavelength λ one can collect signal predominantly from the core or from the Rydberg electron. The compact core will diffract most effectively for x-ray wavelengths in the range λ = 1–10 a.u. (corresponding to photon energies 23–2.3 keV), while the diffuse Rydberg wave function diffracts for $\lambda \gtrsim 10$ a.u., depending on the channel and the principal quantum number n. For small λ, the diffraction from the Rydberg electron is contained at small angles θ and the overall diffraction dominated by the core. Conversely, for large λ the diffraction from the core depends only weakly on the radial angle θ, while the nodal pattern of the Rydberg electron emerges clearly. In Figure 7, at λ = 5 a.u. (4.7 keV) the radial signature of the Rydberg electron, although present, is not readily discernible and the strong signature of the spatial angular distribution dominates the diffraction pattern. At λ = 300 a.u. (78 eV) we see clearly a radial (θ) diffraction pattern corresponding to the nodal pattern of the real-space radial wave function of the Rydberg electron. This pattern does not change much between the two states E_1 and E_2, although it can be distinguished for well-enough matched λ. It is worthwhile pointing out that in most elements, except H and He, the diffraction signal from the core is stronger than from the Rydberg electron. Hence, it may in some situations prove easier to study the Rydberg wave functions indirectly via the

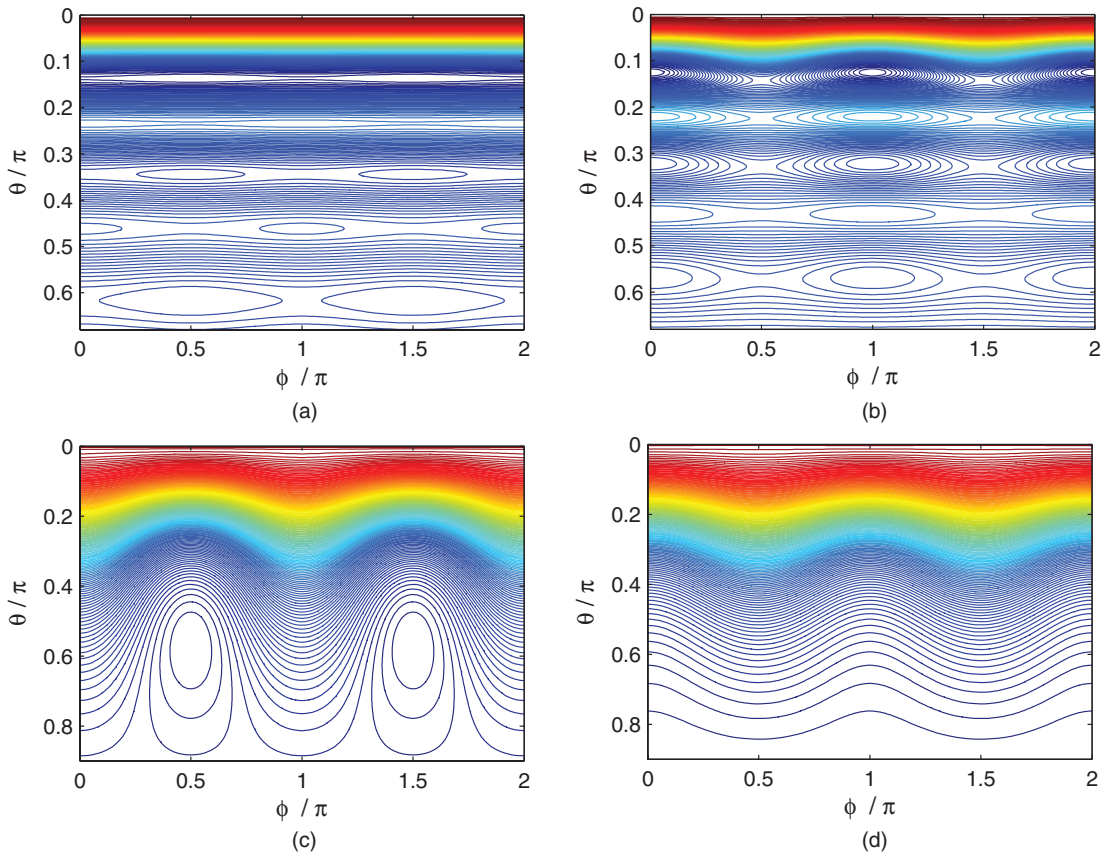

FIG. 7. Contour plots of the diffraction, $|f(\theta, \phi)|^2$, from the Rydberg and the core electrons in Xe atom states E_1 and E_2 (see Table I and Figure 2(b)) for x-ray probe wavelength λ = 5 a.u. (4.7 keV) and λ = 300 a.u. (78 eV). The diffraction angles θ, ϕ are defined in Figure 1. The short wavelength λ = 5 a.u. (bottom row) predominantly probes the core, while λ = 300 a.u. (top row) is more sensitive to the Rydberg electron. The diffraction pattern for state E_1 (left column) is quite different from the pattern for state E_2 (right column), due to the large change in channel populations between the two states, and associated change in spatial angular distribution. (a) State E_1, λ = 300 a.u. (b) State E_2, λ = 300 a.u. (c) State E_1, λ = 5 a.u. (d) State E_2, λ = 5 a.u.

diffraction from the core, rather than to image the Rydberg electron directly.

The preceding discussion demonstrates that it is feasible to distinguish different Rydberg states by their diffraction patterns. However, it should also be possible to characterize each individual state further by fitting a MQDT-derived model to each diffraction pattern. The actual number of parameters that have to be fitted is comparatively small, and a high degree of oversampling is possible in the experiment since diffraction from a large number of unique (θ, ϕ) points can be measured experimentally. In analyzing the diffraction pattern from an experiment one can set up the angular momentum couplings and radial wave functions for each available channel. Such a model can then be used to fit the N_c parameters corresponding to the population in each channel, yielding channel populations and angular momentum compositions from the diffraction pattern. The determination of the radial principal quantum number in each channel requires an additional set of N_c parameters, and x-ray wavelengths that are matched to the radial dimensions of the wave function. The measured data are easier to fit if they extend to comparatively large radial angles θ. For composite Rydberg states with component wave functions with quite different principal quantum numbers it may prove beneficial to measure the diffraction pattern for more than one probe wavelength λ.

V. EXPERIMENTAL CONSIDERATIONS

In an actual experiment, the number of elastically diffracted x-ray photons must be maximized while minimizing background signal due to sample damage and inelastic scattering events. The main parameters are the x-ray pulse characteristics (photon energy, duration, intensity, and focus), the sample volume and density, the excitation scheme, and the efficiency of the detector. Away from absorption edges, the number of diffracted photons is proportional to the product $N_\lambda\, N_{at}\, f_0^2\, \sigma_T$, where f_0^2 is the diffraction amplitude and $\sigma_T = (8\pi/3) r_e^2 = 6.65 \times 10^{-29}$ m the total Thomson cross section with r_e the Thomson radius. Both f_0 and σ_T are intrinsic to the material. On the other hand, the number of incident photons, N_λ, and the number of atoms in the sample, N_{at}, can be maximized in the experiment. Compared to a solid or a liquid, the number of diffracting atoms is small, with the number density for a Rydberg gas scaling approximately as n^{-6} with principal quantum number n. This favours experiments with comparatively small n.

Krause *et al.*[5] estimated the number of diffracted photons per pulse to approximately 10^2, an order of magnitude we essentially agree with. For instance, from a sample of $N_{at} = 10^{14}$ Xe atoms and an x-ray pulse $I_0 = 10^{15}$ W/cm^2, photon energy $E_\lambda = 4.7$ keV and pulse duration $\tau = 100$ fs, with the form factor for the core on the order of $f_0 \sim 10^2$ (17 diffracting core electrons in the outer shell), and $f_0 \sim 1$ for the Rydberg electron, the number of diffracted photons per pulse excluding the isotropic background diffraction from closed inner shell electrons is on the order of 10^2.

At high intensities (e.g., $I_0 \sim 10^{18}$ W cm^{-2} in Ref. 27), multiphoton effects are known to become important. These can be avoided by de-focussing the beam, which keeps the intensity sufficiently low that multiphoton effects do not overwhelm diffraction, while increasing the number of diffracting atoms. Outside the multiphoton regime, the main source of damage is the photoelectric effect. Photoelectric cross sections (attenuation factors) are greater at low energies (soft x-rays), which provide a distinct advantage for hard x-rays. For instance, for Xe atoms $\mu_{PE} = 3.45 \times 10^4$ cm^2/g at $E_\lambda = 79$ eV, while it is $\mu_{PE} = 2.28 \times 10^2$ cm^2/g at $E_\lambda = 4.7$ keV.[28,29] The photoelectric cross sections are also smaller for atoms with few electrons. It seems that the estimates in the paper by Krause *et al.*[5] were somewhat optimistic in not accounting for soft x-ray sample damage.

In order to use Eq. (11) for the analysis of the x-ray scattering signal, experiments should minimize inelastic (Compton) scattering. This favours low-n Rydberg states ($n < 30$) and heavier elements. Compton scattering is also kept small by ensuring that only stationary Rydberg states are excited by using a long duration pulse or CW laser in the excitation scheme and that x-ray pulses with as narrow bandwidth as possible are used (the long life-times of Rydberg states allow comparatively long duration x-ray pulses). The inelastic component becomes more important for x-ray wavelengths $\gtrsim 6$ Å, which again favours low-n Rydberg states or indirect observation of Rydberg states via diffraction from the core. Finally, the Compton scattering may itself contain useful information on the electronic structure of the state, which could be extracted from the experimental data by extending the present theoretical treatment to account inelastic scattering.[26]

Other effects such as nuclear scattering are orders of magnitude weaker. Field ionization of the Rydberg electrons by the oscillating x-ray field is not very efficient, especially for hard x-rays, and in most cases, secondary damage due to, e.g., Auger electrons and inelastic collisions in the sample occur on slower time scales than the duration of the x-ray probe pulse. For instance, avalanche ionization[30] is slower than the typical x-ray pulse duration from a FEL. Most importantly, the proposed experimental setup, with the sample continuously replaced between shots, reduces the effect of secondary damage. Finally, the background diffraction is generally isotropic, while the useful signal is frequently anisotropic due to the alignment by the excitation laser (see discussion in Sec. IV B). This significantly assists with laser-on laser-off image subtraction and improves the signal in the experiment. In the examples discussed in this paper (H and Xe atoms), the M quantum number is well defined in the ground state. In cases where the initial state has a thermal distribution of different quantum numbers M, the Rydberg state carries a corresponding range of M which gives a mixed angular diffraction signal which nevertheless can be fitted.

An alternative route for the experiments proposed in this paper could be to use an electron beam as a probe, instead of x-ray photons.[31–35] Electron diffraction is increasingly becoming a tool for ultrafast dynamics studies,[36] and has the advantage of greater diffraction cross sections than photons. The mathematical form of the operator for electron diffraction is similar to the one for x-ray diffraction in Eq. (10), except that the total charge of the system contributes, including the nucleus. Thus, the ideas and formulas presented in this paper would still largely apply.

VI. CONCLUSIONS

In this paper, we demonstrate the potential utility of x-ray diffraction to identify, distinguish and characterize Rydberg states. The spatial information provided by diffraction could greatly aid spectroscopic assignments. Although we discuss diffraction from H and Xe atoms specifically, Rydberg states in atoms and molecules are very similar,[13] and the results and conclusions can be extended to molecules easily. We calculate diffraction patterns from Rydberg states in H and Xe atoms, and find that the calculated diffraction patterns differ substantially from the isotropic ground state atomic form factors[37] used to fit the positions of atoms in conventional crystallography. In particular, there is a strong spatial anisotropy due to the alignment inferred by the excitation laser, and the subdivision of angular momentum between the core and the Rydberg electron. Angular momentum coupling between the two ensures that the spatial electron distribution of the Rydberg electron is matched by that of the core. For multichannel states of atoms and molecules, rapid changes in character between adjacent states lead to large changes in the spatial angular distribution of electron density. These provide robust signatures in the diffraction pattern, that are not sensitive to the x-ray probe wavelength, and which can be used to distinguish and identify states.

A more detailed characterization of the observed Rydberg states can be obtained by fitting parameters in a theoretical model to the diffraction pattern. In the present paper, we use the MQDT formalism to calculate the electron density and diffraction patterns of excited Rydberg states, thereby providing a unified theoretical framework for both spectroscopy and diffraction, and a direct link between spectroscopy and diffraction-based assignments of the observed states. Using such a model, information about the angular momentum composition, the radial wave functions, and the character of excited electronic states can be extracted from the diffraction. The inherently continuous nature of the diffraction signal (as opposed to crystalline diffraction) provides many unique data points and makes it feasible to fit the relatively modest number of model parameters required for detailed analysis. This is similar to how oversampling of a continuous diffraction permits direct phase retrieval for non-crystalline objects.[38] It is also worthwhile to point out that in some cases, it may prove easier to observe the Rydberg electron indirectly, via diffraction from the many-electron core.

Apart from the intrinsic interest in direct observation of electron wave functions and the utility of unambiguous spectroscopic assignments, it is likely that diffraction techniques will be particularly useful in ultrafast dynamics, to identify transient Rydberg states[10] and provide a time-dependent Rydberg fingerprint spectroscopy.[8] The static treatment of the x-ray scattering used in the current paper is appropriate for Rydberg states, which generally have life times on the order of ps or ns, and it could even be used for slowly evolving Rydberg electron wave packets. However, for very rapidly predissociating molecular Rydberg states or rapidly evolving electron wave packets, where the dynamics occurs in a few fs, it is necessary to account for the quantum electrodynamics of the x-ray scattering[39] because Compton-like transitions become more important. Work is currently underway to extend the present MQDT-based theory to include this situation. It is clear that a successful experiment will have to maximize the number of diffracting atoms in the sample and the number of photons in the pulse, and it is conceivable that more information could be extracted from the experimental signal by including the material response to the electromagnetic field of the x-ray pulse explicitly,[40] especially if high intensity cannot be avoided. Finally, a rather speculative idea is to create a periodic structure to amplify the diffraction signal by trapping Rydberg atoms or molecules in an optical lattice.

ACKNOWLEDGMENTS

The author gratefully acknowledges helpful discussions with Christian Jungen, Niels E. Henriksen, Peter M. Weber, Stephen T. Pratt, and staff and postdoc's at ITAMP, in particular Mikhail Lemeshko. This work was supported by the European Union by grant COCOSPEC (FP7-IEF) and the National Science Foundation through a grant for the Institute for Theoretical Atomic, Molecular and Optical Physics at Harvard University and Smithsonian Astrophysical Observatory. The author is grateful for the hospitality of the African Institute for Mathematical Sciences in Cape Town during early stages of this work.

[1] R. Neutze, R. Wouts, D. van der Spoel, E. Weckert, and J. Hajdu, Nature (London) **406**, 752 (2000).
[2] M. M. Seibert, T. Ekeberg, F. R. N. C. Maia, M. Svenda, J. Andreasson, O. Jönsson, D. Odić, B. Iwan, A. Rocker, D. Westphal, M. Hantke, D. P. DePonte, A. Barty, J. Schulz, L. Gumprecht, N. Coppola, A. Aquila, M. Liang, T. A. White, A. Martin, C. Caleman, S. Stern, C. Abergel, V. Seltzer, J.-M. Claverie, C. Bostedt, J. D. Bozek, S. Boutet, A. A. Miahnahri, M. Messerschmidt, J. Krzywinski, G. Williams, K. O. Hodgson, M. J. Bogan, C. Y. Hampton, R. G. Sierra, D. Starodub, I. Andersson, S. Bajt, M. Barthelmess, J. C. H. Spence, P. Fromme, U. Weierstall, R. Kirian, M. Hunter, R. B. Doak, S. Marchesini, S. P. Hau-Riege, M. Frank, R. L. Shoeman, L. Lomb, S. W. Epp, R. Hartmann, D. Rolles, A. Rudenko, C. Schmidt, L. Foucar, N. Kimmel, P. Holl, B. Rudek, B. Erk, A. Hömke, C. Reich, D. Pietschner, G. Weidenspointner, L. Strüder, G. Hauser, H. Gorke, J. Ullrich, I. Schlichting, S. Herrmann, G. Schaller, F. Schopper, H. Soltau, K.-U. Kühnel, R. Andritschke, C.-D. Schröter, F. Krasniqi, M. Bott, S. Schorb, D. Rupp, M. Adolph, T. Gorkhover, H. Hirsemann, G. Potdevin, H. Graafsma, B. Nilsson, H. N. Chapman, and J. Hajdu, Nature (London) **470**, 78 (2011).
[3] M. R. Pressprich, M. A. White, Y. Vekhter, and P. Coppens, J. Am. Chem. Soc. **116**, 5233 (1994).
[4] M. Ben-Nun, T. J. Martinez, P. M. Weber, and K. R. Wilson, Chem. Phys. Lett. **262**, 405 (1996).
[5] J. L. Krause, K. J. Schafer, M. Ben-Nun, and K. R. Wilson, Phys. Rev. Lett. **79**, 4978 (1997).
[6] H. J. Wörner, U. Hollenstein, and F. Merkt, Phys. Rev. A **68**, 032510 (2003).
[7] H. J. Wörner, M. Grütter, E. Vliegen, and F. Merkt, Phys. Rev. A **71**, 052504 (2005).
[8] N. Kuthirummal and P. M. Weber, Chem. Phys. Lett. **378**, 647 (2003).
[9] K. L. Reid, Annu. Rev. Phys. Chem. **54**, 397 (2003).
[10] S. Deb and P. M. Weber, Annu. Rev. Phys. Chem. **62**, 19 (2011).
[11] T. Suzuki, Annu. Rev. Phys. Chem. **57**, 555 (2006).
[12] R. Neutze, R. Wouts, S. Techert, J. Davidsson, M. Kocsis, A. Kirrander, F. Schotte, and M. Wulff, Phys. Rev. Lett. **87**, 195508 (2001).
[13] C. H. Greene and Ch. Jungen, Adv. At. Mol. Phys. **21**, 51 (1985).
[14] Ch. Jungen, in *Handbook of High-Resolution Spectroscopy*, 1st ed., edited by M. Quack and F. Merkt (Wiley, 2010).
[15] M. S. Child, *Theory of Molecular Rydberg States*, 1st ed. (Cambridge University Press, 2011).
[16] T. F. Gallagher, *Rydberg Atoms*, 1st ed. (Cambridge University Press, 1994).

[17]M. Aymar, C. H. Greene, and E. Luc-Koenig, Rev. Mod. Phys. **68**, 1015 (1996).
[18]U. Fano and A. R. P. Rau, *Atomic Collisions and Spectra*, 1st ed. (Academic, 1986).
[19]K. B. Møller and N. E. Henriksen, Struct. Bond. **142**, 185 (2012).
[20]N. E. Henriksen and K. B. Møller, J. Phys. Chem. B **112**, 558 (2008).
[21]D. McMorrow and J. Als-Nielsen, *Elements of Modern X-ray Physics*, 2nd ed. (Wiley-Blackwell, 2011).
[22]W. C. Martin and W. L. Wiese, "Atomic spectroscopy," in *Atomic, Molecular and Optical Physics Handbook*, edited by G. W. F. Drake (AIP, New York, 1996).
[23]W. R. Johnson, K. T. Cheng, K.-N. Huang, and M. Le Dourneuf, Phys. Rev. A **22**, 989 (1980).
[24]Ch. Jungen and F. Texier, J. Phys. B **33**, 2495 (2000).
[25]C. T. Chantler, K. Olsen, R. A. Dragoset, J. Chang, A. R. Kishore, S. A. Kotochigova, and D. S. Zucker, X-Ray Form Factor, Attenuation and Scattering Tables (version 2.1), available online at http://physics.nist.gov/ffast (NIST, Gaithersburg, MD, 2005).
[26]U. Lorenz, K. B. Møller, and N. E. Henriksen, Phys. Rev. A **81**, 023422 (2010).
[27]L. Young, E. P. Kanter, B. Krässig, Y. Li, A. M. March, S. T. Pratt, R. Santra, S. H. Southworth, N. Rohringer, L. F. DiMauro, G. Doumy, C. A. Roedig, N. Berrah, L. Fang, M. Hoener, P. H. Bucksbaum, J. P. Cryan, S. Ghimire, J. M. Glownia, D. A. Reis, J. D. Bozek, C. Bostedt, and M. Messerschmidt, Nature (London) **466**, 56 (2010).
[28]C. T. Chantler, J. Phys. Chem. Ref. Data **24**, 71 (1995).
[29]C. T. Chantler, J. Phys. Chem. Ref. Data **29**, 597 (2000).
[30]G. Vitrant, J. M. Raimond, M. Gross, and S. Haroche, J. Phys. B **15**, L49 (1982).
[31]D. A. Kohl and E. J. Shipsey, Z. Phys. D **24**, 33 (1992).
[32]D. A. Kohl and E. J. Shipsey, Z. Phys. D **24**, 39 (1992).
[33]N. Böwering, M. Volkmer, C. Meier, J. Lieschke, and M. Fink, Z. Phys. D **30**, 177 (1994).
[34]N. Böwering, M. Volkmer, Ch. Meier, J. Lieschke, and R. Dreier, J. Mol. Struct. **348**, 49 (1995).
[35]J. D. Geiser and P. M. Weber, J. Chem. Phys. **108**, 8004 (1998).
[36]A. H. Zewail, Science **328**, 187 (2010).
[37]R. C. Agarwal, Acta Cryst. **A34**, 791 (1978).
[38]H. N. Chapman, A. Barty, M. J. Bogan, S. Boutet, M. Frank, S. P. Hau-Riege, S. Marchesini, B. W. Woods, S. Bajt, W. H. Benner, R. A. London, E. Plönjes, M. Kuhlmann, R. Treusch, S. Düsterer, T. Tschentscher, J. R. Schneider, E. Spiller, T. Möller, C. Bostedt, M. Hoener, D. A. Shapiro, K. O. Hodgson, D. van der Spoel, F. Burmeister, M. Bergh, C. Caleman, G. Huldt, M. M. Seibert, F. R. N. C. Maia, R. W. Lee, A. Szöke, N. Timneanu, and J. Hajdu, Nat. Phys. **2**, 839 (2006).
[39]G. Dixit, O. Vendrell, and R. Santra, Proc. Natl. Acad. Sci. U.S.A. **109**, 11636 (2012).
[40]H. M. Quiney and K. A. Nugent, Nat. Phys. **7**, 142 (2011).